Mar Geophys Res (2006) 27:289–300
DOI 10.1007/s11001-006-9009-y

ORIGINAL PAPER

Structure of the Malpelo Ridge (Colombia) from seismic and gravity modelling

Boris Marcaillou · Philippe Charvis · Jean-Yves Collot

Received: 27 March 2006 / Accepted: 28 August 2006 / Published online: 2 November 2006

Abstract Wide-angle and multichannel seismic data collected on the Malpelo Ridge provide an image of the deep structure of the ridge and new insights on its emplacement and tectonic history. The crustal structure of the Malpelo Ridge shows a 14 km thick asymmetric crustal root with a smooth transition to the oceanic basin southeastward, whereas the transition is abrupt beneath its northwestern flank. Crustal thickening is mainly related to the thickening of the lower crust, which exhibits velocities from 6.5 to 7.4 km/s. The deep structure is consistent with emplacement at an active spreading axis under a hotspot like the present-day Galapagos Hotspot on the Cocos-Nazca Spreading Centre. Our results favour the hypothesis that the Malpelo Ridge was formerly a continuation of the Cocos Ridge, emplaced simultaneously with the Carnegie Ridge at the Cocos-Nazca Spreading Centre, from which it was separated and subsequently drifted southward relative to the Cocos Ridge due to differential motion along the dextral strike-slip Panama Fracture Zone. The steep faulted northern flank of the Malpelo Ridge and the counterpart steep and faulted southern flank of Regina Ridge are possibly related to a rifting phase that resulted in the Coiba Microplate's separation from the Nazca Plate along the Sandra Rift.

B. Marcaillou (✉) · P. Charvis · J.-Y. Collot
Géosciences Azur, UMR CNRS, IRD, UNSA, UPMC,
OOV, BP48, 06235, Villefranche-sur-mer, France
e-mail: borism@uvic.ca

Present Address:
B. Marcaillou
School of Earth and Ocean Sciences, University of Victoria,
V8W 2Y2, Victoria, BC, Canada

Keywords Malpelo ridge · Galapagos hot spot · Cocos-Nazca spreading centre · Wide angle seismic · Multichanel seismic

Geological setting: tectonic history of the Panama Basin

The Malpelo Ridge is a part of the Cocos-Nazca volcanic province related to the interaction between the Galapagos Hotspot and the regional spreading centres (Hey 1977; Lonsdale and Klitgord 1978). These authors proposed that the earliest stage of regional oceanic spreading started when the old Farallon Plate split into the Cocos and Nazca Plates drifting away along the east-west trending Cocos-Nazca Spreading Centre, (Fig. 1). The Galapagos Hotspot, currently located beneath the Galapagos Archipelago, marks the apex of the V-shaped Cocos and Carnegie Ridges system. These volcanic ridges are commonly related to the influence of the Galapagos Hotspot on the Cocos-Nazca Spreading Centre activity. Magnetic anomalies show that the thickened crusts emplaced near the spreading centre have been drifting away since 22.7 m.y. (Barckhausen et al. 2001) (Fig. 1a). The Cocos and Carnegie Ridges represent the tracks of the Galapagos Hotspot on the Cocos and Nazca Plates respectively (Johnson and Lowrie 1972). The crustal thickness of the Cocos and Carnegie Ridges, inferred from gravity modelling and wide angle seismic data range from 15 to 20 km (Bentley 1974; Sallares et al. 2003; Wade et al. 1977).

The Malpelo Ridge is a bathymetric high, 300 km long and 100 km wide, trending NE-SW, sub-parallel to the Cocos Ridge (Fig. 1b). The top of the ridge is

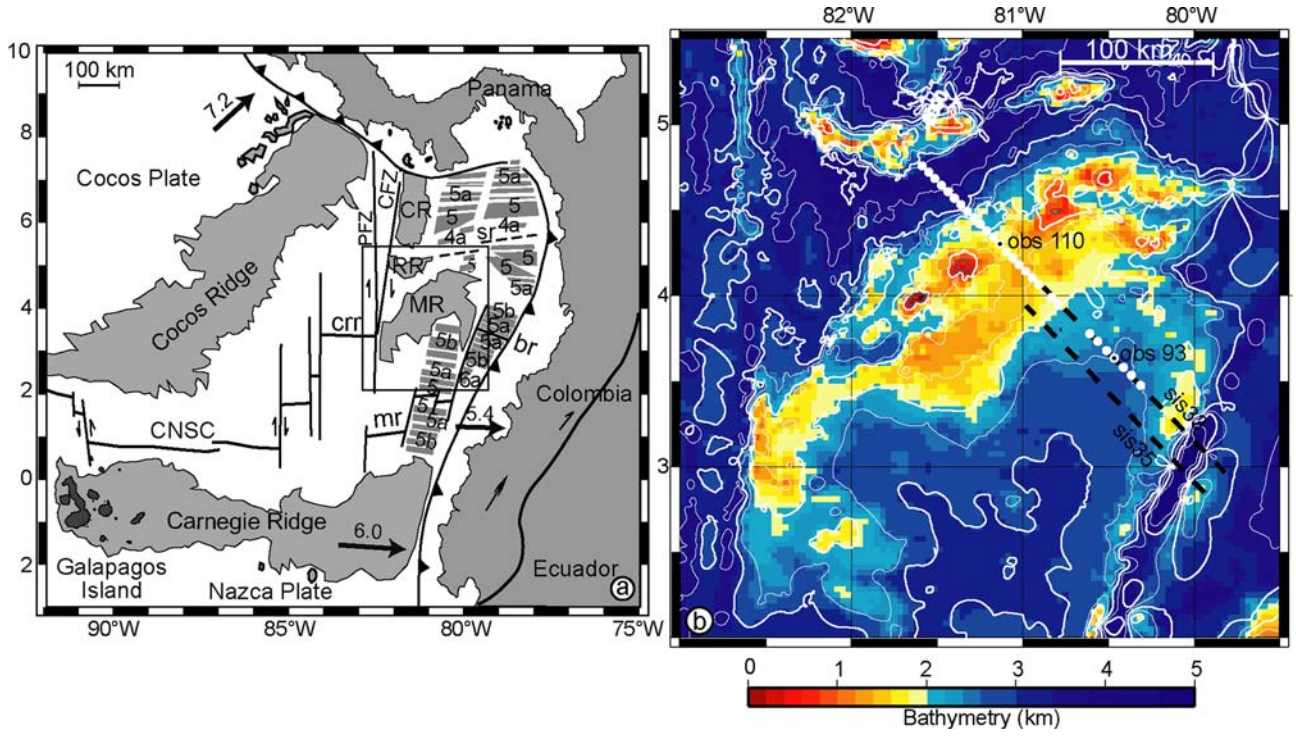

Fig. 1 Location of the study area. **(a)** Structural sketch of the Panama Basin. The major reliefs: Malpelo Ridge (MR), Coiba Ridge (CR), Regina Ridge (RR), Cocos and Carnegie Ridges are shaded in *grey* (limit at 2,000 m depth). *Plain lines* show the major tectonic features: Cocos-Nazca Spreading Centre (CNSC), Costa Rica Rift (crr), Malpelo Rift (mr), Sandra Rift (sr), Coiba Fracture Zone (CFZ) and Panama Fracture Zone (PFZ). Magnetic anomalies are outlined in *grey* (after Barckhausen et al. 2001; Hardy 1991; Lonsdale 2005). *Arrows* indicate absolute plate motion, associated velocities are in cm/y (Kellogg and Vega 1995). The *frame* indicates location of the bathymetric map shown in Fig. 1b. **(b)** Bathymetric map of the Malpelo Ridge (Sandwell and Smith 1997) with the location of the wide-angle seismic line, ocean bottom sensors (*circles*) and multichannel seismic reflection lines Sis-35 and Sis-33 (*dashed lines*). OBSs 110 and 93 shown in Fig. 2 are labelled

1–2 km deep, and is studded with sub-circular highs, interpreted as volcanic edifices; the largest one emerges at the Malpelo Island. These lavas are a late manifestation of the Galapagos Hotspot activity (17.3 ± 0.3 Ma) (Hoernle et al. 2002). The northwestern flank of the Malpelo Ridge shows a ~1,500 m high scarp that contrasts with its gently deepening southeastern flank (Fig. 1b). The Malpelo Ridge has been interpreted as a fragment of the Carnegie Ridge rifted northward during the Malpelo Rift activity, between 17 and 8 m.y. (Hardy 1991; Lonsdale and Klitgord 1978; Pennington 1981). Alternatively, the Malpelo Ridge could rather be the former northward continuation of the Cocos Ridge, shifted southward along the Panama Fracture Zone since 12–9 m.y. (Gardner et al. 1992; Lonsdale and Klitgord 1978; Meschede et al. 1998; Sallares and Charvis 2003).

Magnetic anomalies show that the Malpelo Spreading Centre, started activity, east of the Panama Fracture Zone, 16–17 Ma (Chron 5C) (Lonsdale and Klitgord 1978; Van Andel et al. 1971), ~14.5 Ma (Werner et al. 2003) or ~13.5 Ma (Chron 5A-5) (Lonsdale 2005). Spreading allowed the Carnegie and Malpelo Ridges to separate, similarly to the present-day separation of Cocos and Carnegie Ridges at ~90°W. It is widely accepted that from 12 to 9 m.y., the subduction of the eastern part of the Cocos Plate beneath the Panama Margin was likely plugged by a broadside encounter with the northern counterpart part of the Grijalva scarp (Lonsdale and Klitgord 1978). Most of the authors proposed that the motion of the Nazca Plate, south of Panama, has been taken up along a trench-parallel strike-slip fault since 9 m.y. (Jordan 1975; Molnar and Sykes 1969; Van Andel et al. 1971). This plugging resulted in the opening of a north-south trending major transform fault, the Coiba Fracture Zone (Fig. 1a), and the progressive spreading cessation along the rifts segments located to the east of this fracture zone from 12 to 9.5 Ma (Werner et al. 2003) or 12 to 8–8.5 Ma (Lonsdale and Klitgord 1978; Lonsdale 2005). Since 9 m.y., the Coiba Fracture Zone and then the Panama Fracture Zone have separated two domains of differing tectonic evolution. To the east, the relative position of the Carnegie and Malpelo Ridges remained fixed since the spreading had ceased, while to the west, the Cocos Ridge kept on drifting

away from the Carnegie Ridge (Hey 1977; Lonsdale and Klitgord 1978). Finally, these authors pointed out an E-W trending sinistral shear zone, active since at least 1 m.y., to the north of the Malpelo Ridge and likely coincident with the Sandra Rift (Fig. 1a).

Another geodynamic model based on magnetic reconstruction and seismic studies suggests that the Panama Basin results from three successive spreading phases of the Cocos-Nazca Spreading Centre, starting 23 Ma, and separated by ridge jumps at ~19.5 and 14.5 m.y. (Barckhausen et al. 2001; Meschede et al. 1998). During this period the excess melt flux beneath the Cocos and Nazca Plates was related to the varying distance between the spreading centre and the Galapagos Hotspot (Werner et al. 1999).

In this paper, we propose a crustal model for the Malpelo Ridge, inferred from recently acquired wide-angle and multichannel seismic reflection data and satellite-borne gravity anomalies. We then discuss the evidences of volcanic origin for the ridge, related to the interaction between a hotspot and a spreading centre. We also examine new evidence for the ridge tectonic evolution bearing on its crustal structures and relationships with Regina, Cocos and Carnegie Ridges.

Data analysis and modelling

Wide angle seismic data

During the Paganini experiment (1999) on board the German R/V SONNE (Bialas et al. 1999), a 244 km long wide-angle seismic line was shot across the Malpelo Ridge, using three 32 l airguns as seismic source. Altogether 33 ocean bottom instruments (OBS) equipped with 3–components seismometers and/or hydrophones were deployed along this line (Fig. 1b). The seismic record sections show clear arrivals from the crust and the upper mantle, traced up to 180 km. The data mainly exhibit refracted waves in the upper igneous crust (P1), in the lower crust (P2), and in the upper mantle (Pn) and reflected waves from the Moho (PmP) (Fig. 2). A preliminary velocity model was first constructed on the basis of the simultaneous inversion of first arrivals (P1 and P2) and PmP arrivals (Sallares et al. 2003) (see Malpelo Ridge emplacement). This model exhibits an up to 19 km thick crust with a layer 2 of uniform thickness, whereas thickening is mainly accommodated by layer 3. Our new Malpelo Ridge velocity model is derived from forward modelling and 2D iterative damped least square inversion of travel times of refracted and reflected waves (Zelt and Smith 1992).

Model uncertainty

We assess the quality of the final velocity model using Root Mean Square (RMS) values (Table 1) which characterize the generally close agreement between observed and calculated travel times (Fig. 2) related to ray coverage (Fig. 3a). The global RMS misfit for the model is 0.1 s and ranges, for individual layer, from 0.06 s for the upper crust to 0.15 s for the mantle which is comparable to phase picks uncertainties (Table 1). Moreover the RMS value for each node of the model shows that the highest misfits are essentially located along the Moho at the limits of the line: km 0–60 (OBS 117–122) and km 200–244 (OBS 90–95) (Table 1). These sections are poorly constrained because of a low number of ray hits (Fig. 3a). It is noteworthy that the section of interest of the Moho in this paper is located between km 60 and 180 (OBS 96–116) which is constrained by a much higher resolution (except for the shadow zone at km 90–100) (Fig. 3a). For this central part of the model the global RMS misfit is 0.08 and for individual layer ranges from 0.04 for the upper crust to 0.1 for the Mantle (Table 1). Thus the resolution and uncertainties of the model are globally good. Moreover the highest potential errors, in Moho depth and/or mantle velocities, are located at the limit of the model and then would have a low influence on the Moho geometry and mantle velocity beneath the ridge axis and flanks, which are the focus of this paper.

Velocity model

The 244 km long velocity model (Fig. 3), with an origin corresponding to the northwestern end of the wide-angle line, consists of three layers from top to bottom.

Because of the lack of arrival refracted in the sedimentary cover, we assumed for this layer a seismic velocity of 1.8 km/s, consistent with velocity analysis along multichannel seismic lines in the area. Its thickness inferred from the refraction (P1) in the upper igneous crust (Fig. 2) is highly variable from zero on top of basement highs to ~1.2 km in small basins defined by basement lows, and in the southeastern half of the profile (Fig. 3). Moreover, a multichannel seismic line, SIS-33, parallel to the line SIS-35 is coincident with the wide angle line, between km 110 and km 240 (Fig. 1). The sedimentary cover thicknesses calculated on this seismic line are closely consistent with our estimations (Agudelo 2001; Agudelo et al. 2002). In this paper we mainly use seismic line SIS-35 which presents a better signal/noise ratio in the crust.

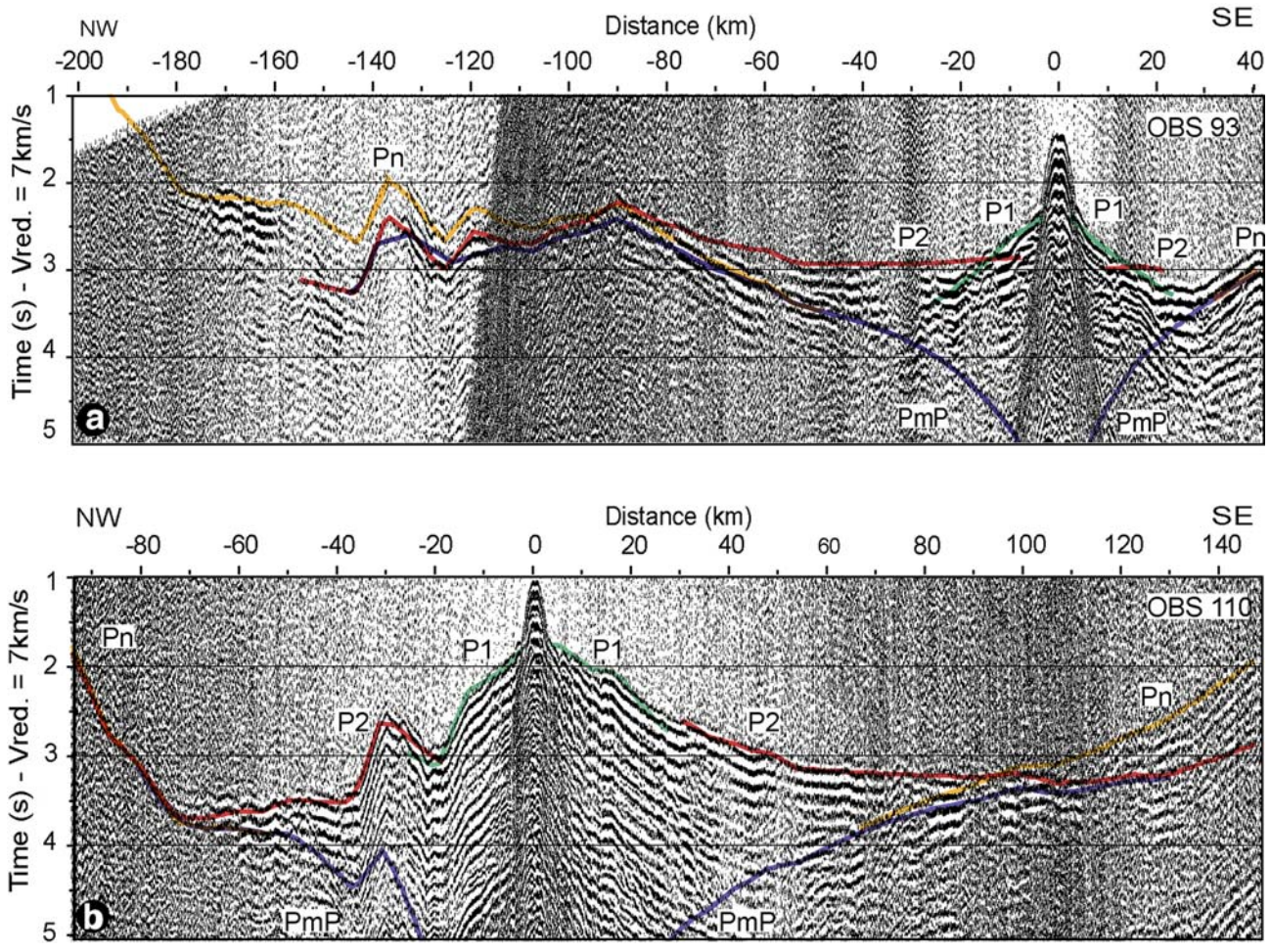

Fig. 2 Wide-angle seismic sections. **(a)** OBH record section 093 and **(b)** OBS record section 110 (location in Fig. 1). Reducing velocity is 7 km/s. Computed travel times in the final velocity model (Fig. 3b) are shown for comparison: refraction in the upper igneous crust (P1), refraction in the lower crust (P2), refraction in the upper mantle (Pn) and reflection from the Moho (PmP)

Table 1 Observed phases and travel time fits for the final model (Fig. 3)

Layer	Phase	OBS	Pick uncertainty	RMS misfit
Upper crust	P1	A+B	0.05	0.06
Lower crust	P2	A+B	0.08	0.1
Lower crust	P2	B	0.08	0.08
Mantle	Pn	A+B	0.1	0.12
Mantle	Pn	B	0.1	0.1
Mantle	PmP	A+B	0.2	0.15
Mantle	PmP	B	0.2	0.1

Note that Root Mean Square (RMS) misfits between calculated and observed travel-time are comparable to pick uncertainties. We divide the OBS pool in two categories: A/OBS located beneath the central part of the model (96–116) and B/OBS located beneath the limit of the model (117–122 and 90–95). This highlights that the highest RMS misfits are concentrated at the limits of the models, the RMS values are much lower beneath the central part of the model which is the focus of this paper

The velocities in the upper igneous crust, constrained by refraction P1, range from 4.9–5.1 km/s at the top of the upper igneous crust to 5.8–6.1 km/s at its bottom. Its thickness varies gently across the ridge, from 4 km at km 60, to 3 km at km 240, and is less than 1.8 km to the north of the ridge, from km 20 to km 60 of the profile (Fig. 3).

In the lower crust, seismic velocities range from 6.6–6.9 km/s at its top to 7.1–7.5 km/s at its base (Fig. 3b). Beneath the Malpelo Ridge, the lower crust thins from ~16 km at km 110, to ~6 km at the south-eastern end of the profile (Fig. 3b). Between km 40 and km 60 the lower crust is 10 km thick.

The Moho, constrained by PmP and Pn, reaches a depth of ~22 km below the shallowest part of the ridge top, and ~14 km at both ends of the seismic profile. Its shape is highly asymmetric, rising with a 5° angle to the southeast and with 14° angle to the northwest end of the line. Pn arrivals, refracted in the upper mantle are

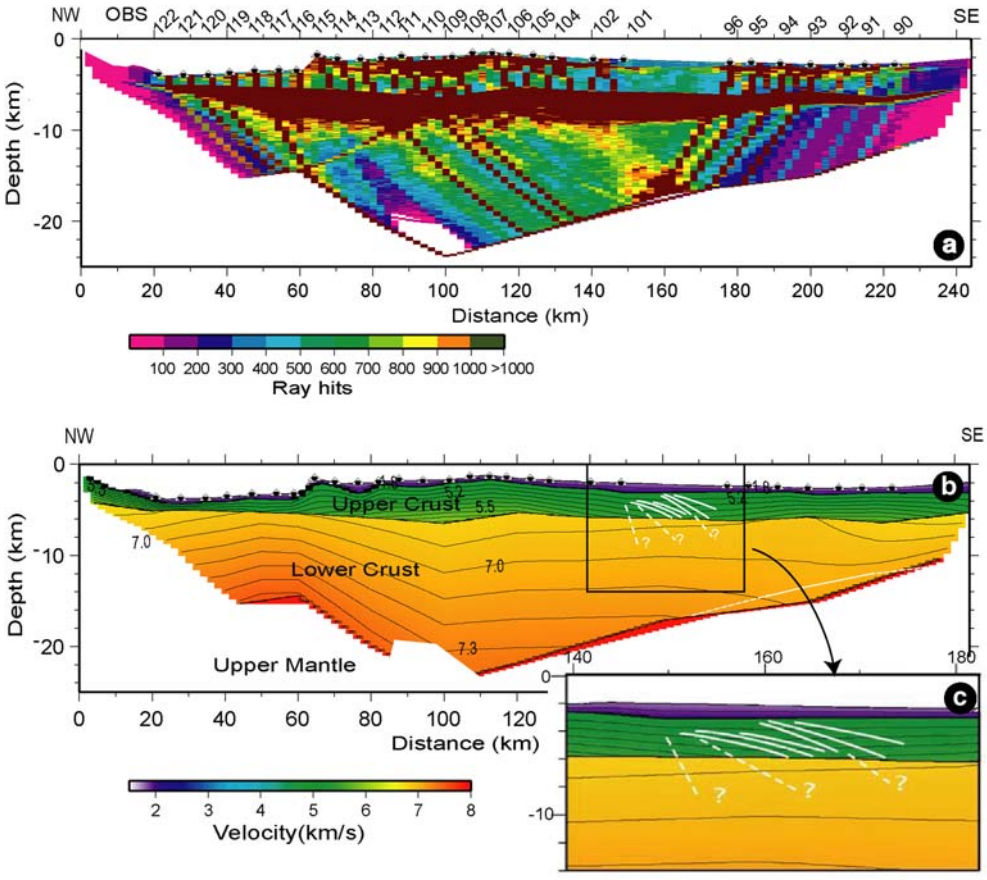

Fig. 3 Velocity model of the Malpelo Ridge obtained from wide-angle seismic data. **(a)** Number of rays travelling in the model for the final velocity model shown below. A large number of rays allow a better constraint on the model. Structures in the deep crust are well constrained for distances ranging from 50 to 180 km. **(b)** Final velocity model. Seismic velocities are *colour coded* and *contoured*. The Moho and some dipping reflectors inferred from multichannel seismic line SIS-35 (Fig. 1b) are shown in *white*. **(c)** Zoom showing the dipping reflectors interpreted from multichannel seismic data. Most reflectors are confined into the layer 2 and present a gentle upward convexity and a fan organization. *Dashed lines* outline weak rectilinear reflectors crosscutting the layer 2-layer 3 boundary

only reversed at the Moho between km 120 and 180. They are consistent with a uniform velocity of 7.9 km/s in the upper mantle.

Gravity modelling

The velocities for each layer of the velocity model were converted into crustal density according to empirical relations. Because of low lateral velocity variation within each layer of the seismic model, they were assumed to be bodies with a uniform density except for the lower crust, which was modelled as two distinct bodies. The sediment velocity, set to 1.8 km/s, corresponds to density of 1.9 g/cm^3 (Carlson and Raskin 1984) or 2.0 g/cm^3 using the relation for shale $\rho = 0.917 + 0.747\text{Vp} - 0.08\text{Vp2}$ (Hamilton 1978). The upper crust, with seismic velocities ranging from 4.9 to 5.1 km/s at the upper boundary and from 5.8 to 6.1 km/s at the lower boundary, was modelled as a body of uniform density 2.6 g/cm^3 (Carlson and Raskin 1984). The more recent empiric relation, $\rho = 3.61 - 6.0/\text{Vp}$, provide for these seismic velocities, similar densities ranging from 2.5 to 2.6 g/cm^3 (Carlson and Herrick 1990). The lower crust was divided into two distinct bodies. Using the Carlson and Raskin (1984) relation, the uppermost part (Vp from 6.6 to 7.1 km/s) and the lowermost part (Vp from 7.1 to 7.5 km/s) were modelled as bodies with respective densities 2.9 and 3.0 g/cm^3. A older velocity-density relation for plagioclase and diabase-gabbro-eclogite, $\rho = 0.375 + 0.375\text{Vp}$ (Birch 1961), which is considered to be more adequate to model the oceanic lower crust, provide exactly the same results. Gravity anomalies computed along the 2D-crustal model using the method of Talwani et al. (1959), were then compared to satellite-borne free-air gravity anomalies (Sandwell and Smith 1997) (Fig. 4). It is noteworthy that satellite data without control from shipboard gravity data are efficient to model long-wavelength anomalies but have some quality limitations to model the short-wavelength anomalies as discussed below.

To achieve the fit of the long-wavelength anomalies (>30 km), either the crustal thickness must be increased in the southeastern part of the model (km 160 to 244), or the density of the upper mantle slightly decreased across the profile (0.05). As the Moho is properly constrained by the seismic refraction data (Fig. 3) but also by multichannel seismic data (next paragraph), we

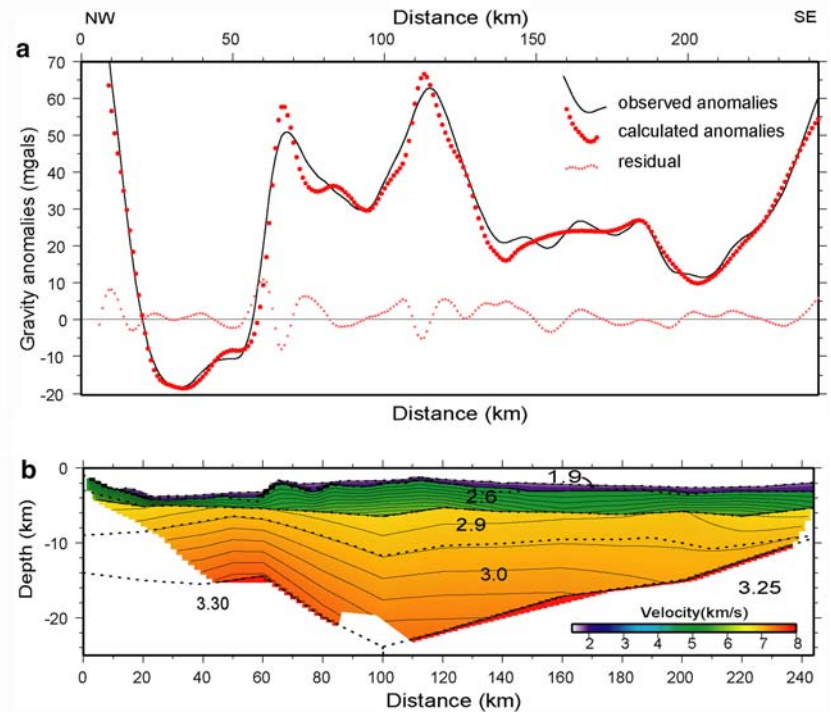

Fig. 4 Gravity model of the Malpelo Ridge obtained from satellite-borne free-air gravity anomalies. **(a)** Observed and calculated Free Air gravity anomalies. **(b)** Densities, in g/cm^3, used for gravity modelling are indicated. *Dashed lines* marking the limit of bodies used for gravity modelling overlay the refraction velocity model (Fig. 3b). The origin of the model corresponds to the northwestern end of the wide-angle line

choose the second hypothesis and allow the density of the upper mantle to decrease from 3.30 g/cm^3 in the northwestern part (km 0–100) to 3.25 g/cm^3 in the southeastern part (km 100–244) (Fig. 3b). Some adjustment of the basement topography (upper crust, Fig. 3b) was also necessary to improve the fit of short wavelength anomalies (~10–20 km). The final fit is good, only short wavelength discrepancies, between 5 and 10 mgal appear on the residual curve (Fig. 4). These discrepancies are mainly located along the northwestern flank and the crest of the ridge (km 0–140). This part of the wide-angle model is not constrained by multichannel seismic data suggesting that the discrepancies are likely related to the poorly constrained topography of the basement. The discrepancies along the crest of the ridge may also be due to possible 3D effects related to volcanic edifices on the top of the ridge.

Multichannel seismic reflection data

During the SISTEUR experiment on board the R/V NADIR (Collot et al. 2002) a 360-channel seismic reflection profile, SIS-33, was shot across the southern flank of the Malpelo Ridge, coincident with the PAGANINI wide-angle seismic line between km 110 and km 240 (Fig. 1). A second multichannel seismic line, SIS-35, with a better signal to noise ratio, located ~20 km southward and parallel to the previous one is used to illustrate the Malpelo Ridge structure (Figs. 1, 5a). In this figure These 45-fold seismic data were recorded using a 45 l airgun seismic source tuned in single-bubble mode and a 4.5 km long streamer.

Seismic lines were processed using the Geovecteur® software package with the following sequence: (1) conversion of the data into minimum phase and deconvolution, (2) gain restitution by an accurate velocity analysis, (3) anti-multiple, performed in the FK domain, and by an internal mute of the first multiple, (4) normal and deep move out, (5) Stack, and (6) a Kirchoff migration. This processing sequence improved significantly the signal to noise ratio and allows some important patterns to be identified.

The southeastern part of the seismic reflection profile exhibits a discontinuous, low frequency reflector at 7–7.5 s two-way time (Fig. 5b). According to the crustal velocity structure, derived from refraction modelling, this reflector is consistent, in dip and general depth, between 11 and 17 km, with the refraction-derived Moho, although the later departs locally from the former by ~1 km (Fig. 3b).

A 60 km long segment of the seismic reflection line also exhibits SE-dipping crustal reflectors. Most are very discrete features, except along a 22 km long segment of the profile, where they show relatively strong amplitudes (Fig. 5b). The dipping reflectors were depth-converted using the velocity model constructed from the wide-angle seismic data. The dipping reflec-

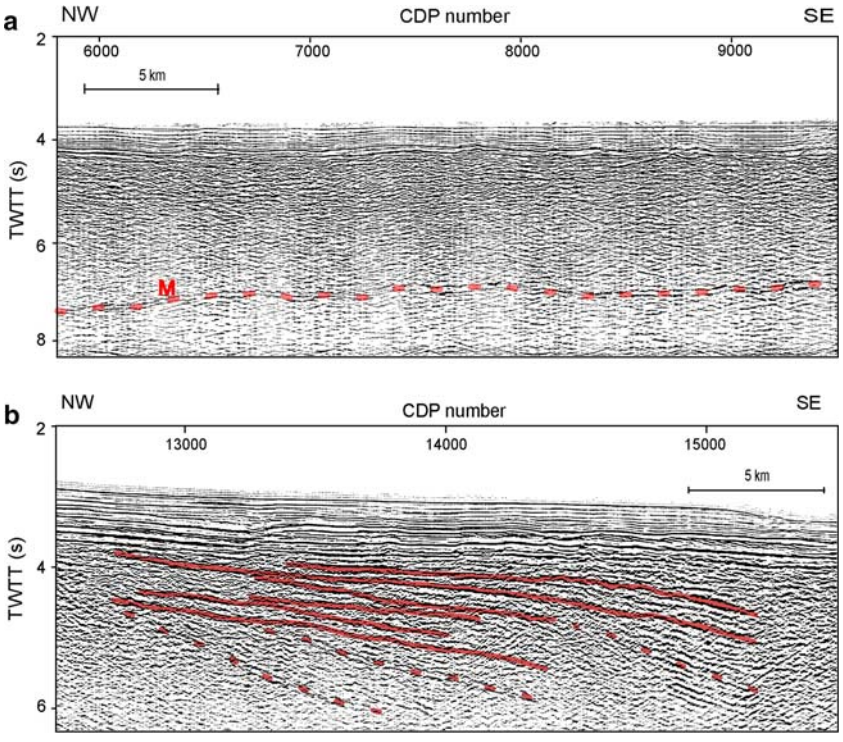

Fig. 5 Close-ups of the multichannel seismic reflection line SIS-35 (location in Fig. 1b). **(a)** Deep reflection M likely related to the Moho (see Fig. 3b for location in depth). **(b)** Dipping reflectors with a fan organization and a gentle upward convexity are interpreted as lava flows. The rectilinear reflectors (*dashed lines*), extending down to 5–6 s two-way travel time with a steeper dip, are interpreted as crustal faults. The interpreted reflectors were depth converted and displayed in the Fig. 3b

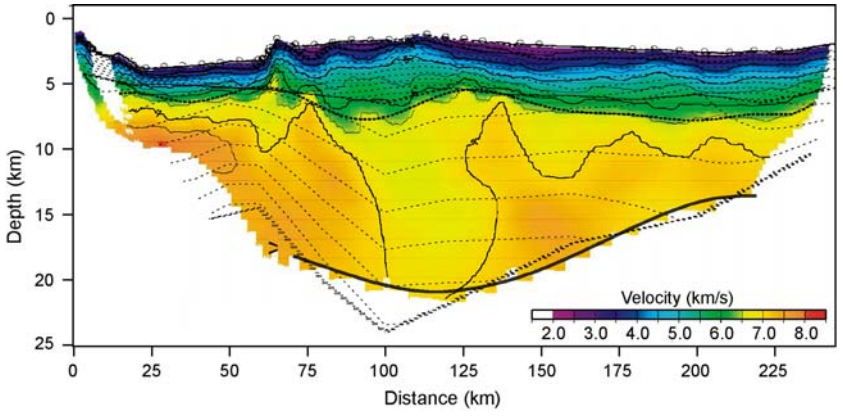

Fig. 6 Wide angle model of the Malpelo Ridge from Sallares et al (2003). The isovelocities lines (*dotted lines*) derived from our model highlight the consistency of both models. The origin of the models corresponds to the northwestern end of the wide-angle line

tors (Fig. 5b) exhibit a gentle upward convexity. They are nearly horizontal at their upward extremity and dip downward from 11 to 20° (Fig. 3). This geometry gives an overall wedge-shaped appearance to the reflector sequence without clear basal termination. Some weak and rectilinear reflectors dipping southeastward with an angle of ~30°, may crosscut the layer 2-layer 3 boundary (Fig. 3b).

Interpretation

Malpelo Ridge emplacement

The layered model obtained in this study and the tomography model from Sallares et al. (2003), based on the same data set, are very much consistent (Fig. 6).

- The main sedimentary basins at km 75, 100 and 150 appear clearly on both models.
- The base of the upper crust (layer 2) in our model coincides with isovelocity 6.0 km/s in the tomography model. Both models exhibit a thinning of the layer 2, from 5 to 2 km, between km 20 and km 60 (Fig. 3).
- Our approach, based on the use of both PmP and Pn arrivals provide a better constrained on the Moho, except from km 40 to km 80, where the Moho depth varies from 15 km, beneath the ocean basin north of the ridge, to 20 km beneath the top of the ridge. From km 125 to km 225 on both models, the Moho rises gently from 22 to 12 km depth.

- The velocity in the lower crust (layer 3) is similar in both models (isovelocity 7.0 km/s coincides) except in the central part of the model (km 100–123), where our model shows a lower crustal velocity up to 7.3 km/s down to the Moho, whereas in the tomography model the velocity remains as low as 7.0 km/s. Nevertheless our model shows that the highest seismic velocity is reached beneath the northern part of the model where the crust is only ~10 km thick as discussed by Sallares et al. (2003).

The crust of the Malpelo Ridge reaches a maximum thickness of 21 km, whereas the surrounding oceanic crust is 11 km thick north of the ridge and ~10 km thick southeast of it (Fig. 3b). Because the thickness of the upper igneous crust remains sub-constant (3–4 km), the ~11–13 km ridge crustal thickening, appears to result directly from thickening of the lower crust, which reaches 10–12 km (Fig. 3b). Seismic velocities are consistent with volcanic lava flows for the upper igneous crust (5.0–5.7 km/s) and reach 7.5 km/s at the base of the crust. Such a velocity structure is commonly found in oceanic plateaus (Coffin and Eldholm 1994; Mutter and Mutter 1993) despite the fact that the maximum seismic velocity (7.4 km/s) is observed in the lower crust at km 40–60 of the model and not where the crust reaches its maximum thickness (at 100 km). Sallares et al. (2003) showed that this feature is also observed along wide-angle lines sampling the Cocos Ridge and suggested this could be related to a mantle melting dominated by moderate to vigorous upwelling or heterogeneities in the mantle source. The two-layer igneous crust does not show any marked seismic discontinuity between the upper and lower crustal layers, but only a change in the velocity gradient. These findings support a magmatic emplacement in a context of interaction between an active hotspot and a spreading centre, as described in Iceland (Bjarnason et al. 1993), on the Kerguelen Plateau (Charvis and Operto 1999; Charvis et al. 1995) and in other similar settings (Mutter and Mutter 1993).

Basement dipping reflectors are commonly described in areas affected by extensive volcanism such as oceanic plateaus (Schlich et al. 1993), volcanic margins (Callot et al. 2001; White 1992), and oceanic crust (Banda et al. 1992; McCarthy et al. 1988; White et al. 1994). Two models of emplacement of the dipping reflectors are proposed: (1) an isostatic model assuming that fan-shaped convex dipping reflectors in the upper crust result of a progressive flexure of the lavas towards the ridge due to differential loading by the newly erupted flows (Eldholm 1991; Hinz 1981; Mutter 1985; Mutter et al. 1982; Palmason 1980); (2) a tectonic model interpreting rectilinear reflectors cross-cutting the whole crust, or part of it, as faults (Barton and White 1997; Geoffroy et al. 1998; Tard et al. 1991).

On the multichannel seismic line, most of the southeastward dipping reflectors are confined to the upper crust. They are associated in fan-shaped sequences and show an upward convexity, which are typical features of reflectors related to progressive flexure of the lavas, as described by the isostatic model (1). Thus on the southeastern flank of the Malpelo Ridge, these fan-shaped reflectors ensconced in layer 2 likely reflect lavas flows flexure due to the proximity of the ancient spreading centre, under a high rate of magmatism. The Late Miocene interaction of the Cocos-Nazca Spreading Centre and the Galapagos Hotspot provided this setting (Sallares and Charvis 2003). Nevertheless some dipping reflectors (in dashed lines Figs. 3c, 5b) cut across the layer 2-layer 3 boundary as described in the tectonic model (2). Then these rectilinear reflectors are consistent with low-angle faults described in previous studies (Banda et al. 1992; McCarthy et al. 1988) and rather reflect the tectonic evolution of the southeastern flanks of the Malpelo Ridge. They are not associated with offsets of the basement top, possibly because intense volcanism masked shallow tectonic effects associated with the ridge formation (McCarthy et al. 1988).

The thickened crust of the ridge associated with lavas flows dipping toward the former spreading centre are consistent with an emplacement of the Malpelo Ridge, on the northern flank of the Cocos-Nazca Spreading Centre, under the influence of a high rate of magmatism provided by the Galapagos Hotspot during the Late Miocene. We propose, as described below, that the rectilinear reflectors cross-cutting the layer 2-layer 3 boundary, likely low angle fault planes, reflect the later tectonic evolution of the southeastern flank.

Malpelo Ridge tectonic evolution

Magnetic anomalies show that the spreading in the Panama Basin ceased 9–8 Ma (Lonsdale and Klitgord 1978; Werner et al. 2003). A recent magnetic re-interpretation suggests that the spreading ceased along the Malpelo Rift shortly after 9 my but continued along the Sandra Rift (Fig. 7), maybe until 8.5 my (Lonsdale 2005). This interpretation suggests that the Sandra Rift was a Cocos-Nazca spreading axis that propagated westward from at least 12 Ma to ~9 Ma overlapping the concurrently spreading eastern segment of Malpelo Rift where spreading slowed after 12 my. Since this period, the Sandra Rift has possibly been rejuvenated

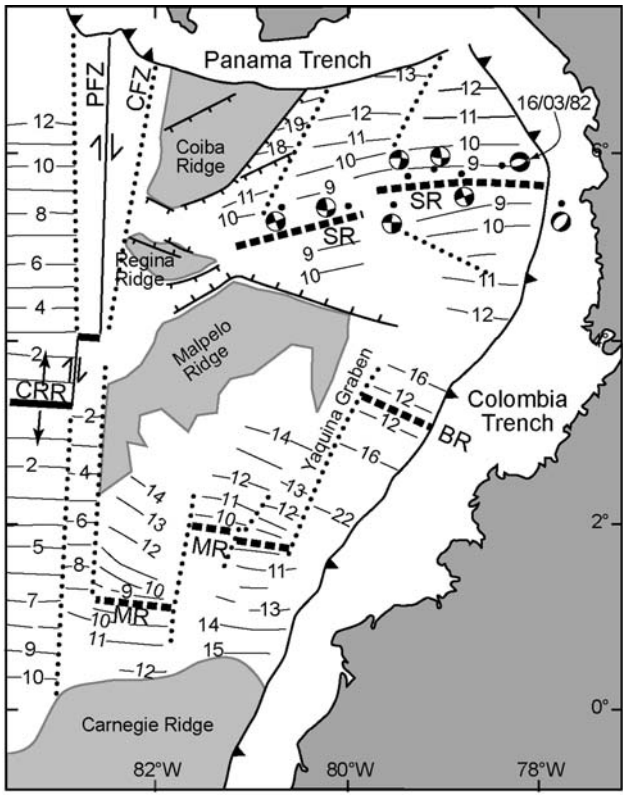

Fig. 7 Interpretation of the pattern of crustal isochrons (Hardy 1991; Lonsdale 2005) and plate boundaries in the Panama Basin (modified from Lonsdale 2005). Earthquakes (*black dots*) and fault plane solution are from the Harvard University archive of centroid-moment tensor solutions. *Plain lines* are active spreading axis and transform faults: Costa Rica Rift (CRR) and Panama Fracture Zone (PFZ). *Dashed* and *dotted lines* are fossil spreading axis and transform faults: Buenaventura Rift (BR), Malpelo Rift (MR), Coiba Fracture Zone (CFZ) and Yaquina Graben. Possible spreading activity along Sandra Rift (SR) is still in discussion

at times by tension resulting from slab pull forces acting in different directions due to the curvature of the Colombian trench (Hardy 1991). Moreover, this rift is still marked by a band of seismicity supporting residual or reactivated tectonism (Fig. 7). Some authors proposed that a spreading reactivation along the Sandra Rift may has partially caused a reactivation of a slow northeast-directed subduction beneath Panama, possibly since 3–5 Ma (de Boer et al. 1988; Silver et al. 1990). Several normal-faulting focal mechanisms along the Sandra Rift (as the 16/03/82 event) implying a rifted ''not-quite-abandonned'' spreading axis, support this hypothesis. Alternatively, other authors pointed out an E-W trending sinistral shear zone, coincident with the Sandra Rift and active since at least 1 my (Adamek et al. 1988; Hey 1977; Lonsdale and Klitgord 1978; Sallares and Charvis 2003). Most of the centroid moment tensor solutions along the Sandra Rift indicate strike-slip focal mechanism (Lonsdale 2005) consistent with a sinistral shear zone. This shear zone is thought to be the southern boundary of the Coiba Microplate which have a slightly different motion than the Nazca and Cocos Plates (Lonsdale and Klitgord 1978). According to these authors the separation of this microplate from the Nazca plate, altogether with a westward jump of the Caribbean-Nazca-Cocos triple junction and a westward jump of the transform fault from the nowadays fossil Coiba Fracture to the Panama Fracture Zone, occurred during a recent rifting phase, likely less than 5 Ma (Sallares and Charvis 2003). Most of the geodynamic models suggest that the Malpelo and Regina Ridges split and drifted away while these recent tectonic events, but the mechanism of this division remains unclear. The Malpelo-Regina Ridges separation may be related to the spreading activity along the Sandra Rift, similarly to the present-day separation of Cocos and Carnegie Ridges at ~90°W, and possibly occurred before the spreading cessation, 12–9 Ma or during a recent reactivation. Alternatively the Malpelo-Regina Ridges separation may be related to the recent rifting phase that created the Coiba Microplate.

The strong asymmetry of the Moho of the ridge mirrors the seafloor and basement topography, suggesting that the crustal evolution of northwestern and southeastern flanks of the ridge was controlled by processes of different nature. The progressive southeastward Moho shallowing, from km 110 to 240, matches with a gentle seafloor and basement deepening. The sharp northeast Moho rise from km 100 to 60 coincides, near km 60–80, with major seafloor or basement northeast-facing scarps supporting the dominant influence of tectonics at the ridge northeast flank. The crust thinning process also differs beneath the northern and southern flanks, as indicated by the relative variations in thickness of the upper and lower crusts. To the southeast, the ridge thinning is mostly accommodated by layer 3 thinning from 18 to 6 km, whereas layer 2 thins only from 4 to 3 km. To the northwest, from the ridge summit to the 12 km thick oceanic crust north of the ridge, thinning of layer 2, (~2.5-fold) is larger than thinning of layer 3 (1.7-fold). Changes in magmatic activity are known to generate large thickness variations of crustal layer 3 and only little variation of crustal layer 2 (Mutter and Mutter 1993). Therefore, the subdued southern flank, which exhibits dipping reflectors and a strong thinning of the crustal layer 3, suggests initial ridge construction by extensive hotspot volcanism near the active spreading axis and a progressive decrease in magmatic activity when the active spreading centre drifted away from

the hotspot. We propose that the low-angle dipping reflectors cross-cutting the layer 2-layer 3 boundary are fault planes reflecting this progressive drifting of the Malpelo Ridge from the hotspot and the related decrease of magmatic supply. The Malpelo Ridge drifted until that the spreading along the Malpelo and/or Sandra spreading axis ceased 9.5 Ma (Werner et al. 2003), 9–8.5 Ma (Lonsdale 2005) or 8 Ma (Lonsdale and Klitgord 1978). The steep and faulted northern flank of the Malpelo Ridge faces the sharp and likely faulted southern flank of the Regina Ridge. Moreover the crustal thinning is not mainly supported by a progressive decrease of the layer 3 thickness, as beneath the southeastern flanks, but by a drastic and abrupt thinning of both crustal layers and especially the layer 2. These features are inconsistent with a Malpelo-Regina Ridges separation by a spreading activity and suggest that the ridges were more likely separated by a rifting process. This tectonic phase possibly relates to the rifting phase that created the Coiba Microplate and has occurred since 8 my (Lonsdale and Klitgord 1978; Taboada et al. 2000) or 5 my (Sallares and Charvis 2003). In this hypothesis, the oceanic basin ensconced between Regina and Malpelo Ridges is likely underlain by stretched ridge crust thus accounting for layer 2 thinning. Then these results clearly favour the hypothesis that the Malpelo Ridge was formerly the continuation of the Cocos Ridge, emplaced simultaneously with the Carnegie Ridge at the Cocos-Nazca Spreading Centre, separated and drifted southward relative to the Cocos Ridge by differential motion along the dextral strike-slip Coiba and Panama Fracture Zones since 12–9 my. The separation between Malpelo and Regina Ridges may be due to a recent rifting phase possibly related to the Coiba Microplate separation from the Nazca Plate.

Conclusions

Wide-angle and multichannel seismic reflection data provide new insights on the origin and history of the Malpelo Ridge.

The Malpelo Ridge exhibits an asymmetric thickened oceanic crust with fan-shaped dipping reflectors consistent with emplacement at an active spreading axis with an anomalously high rate of magmatic production. The Late Miocene interaction of the Cocos-Nazca Spreading Centre and the Galapagos Hotspot provided this setting. The structure of the Malpelo Ridge suggests that the northwestern and southeastern flanks of the ridge underwent different tectonic histories. The southeastward smooth transition from the ridge to the ocean basin, as well as fan-shaped sequence of seaward dipping reflectors within the upper crust support an initial ridge emplacement at the active Malpelo spreading centre. Subsequently the Malpelo Ridge drifted away from the Carnegie Ridge in a similar fashion to the present-day emplacement of the Cocos and Carnegie Ridges at 90°W. The dipping reflectors cross-cutting the layer 2-layer 3 boundary are likely tectonic features, such as low angles fault planes, related to this progressive evolution. The steep northwestern flank of Malpelo Ridge as well as the steep southern one of Regina Ridge reflect intra-plate rifting activity. This latest tectonic phase gave birth to the Coiba-Nazca Plate boundary that is presently reactivated by sinistral shearing. Thus, these new results support a model proposing that the Malpelo Ridge was formerly the continuation of the Cocos Ridge, emplaced simultaneously with the Carnegie Ridge at the Cocos-Nazca Spreading Centre and separated from the Cocos Ridge northern termination by differential motion along the dextral strike-slip Coiba and Panama Fracture Zones.

Acknowledgment The R/V Sonne, supported by the Bundesministerium for Forschung und Technologie was the vessel for data acquisition. We acknowledge the PAGANINI crew, scientific party and the cruise chief: Ernst R. Flueh and Jörg Bialas. We also thank David Graindorge for his helpful review of an early version of this manuscript and exchange of ideas.

References

Adamek S, Frohlich C, Pennington WD (1988) Seismicity of the Caribbean-Nazca boundary: constraints on microplate tectonics of the Panama region. J Geophys Res 93:2053–2075

Agudelo W (2001) La marge convergente sud-ouest Colombienne : structure et déformation à partir de données de sismique multitrace et grand-angle, Rapport de DEA thesis, Pierre et Marie Curie, Villefranche sur mer

Agudelo W, Charvis P, Collot J-Y, Marcaillou B, Michaud F (2002) Structure of the Southwestern Colombia convergent margin from the Sisteur seismic reflection-refraction experiment, in *EGS XXVII*, Nice, France

Banda E, Ranero CR, Dañobeitia JJ, Rivero A (1992) Seismic boundaries of the Eastern Central Atlantic Mesozoic crust from multichannel seismic data. Geol Soc Am Bull 104:1340–1349

Barckhausen U, Ranero CR, von Huene R, Cande SC, Roeser HA (2001) Revised tectonic boundaries in the Cocos Plate off Costa-Rica: implications for the segmentation of the convergent margin and for plate tectonic models. J Geophys Res 106:19207–19220

Barton AJ, White RS (1997) Volcanism on the Rockall continental margin. J Geol Soc London 154:531–536

Bentley LR (1974) Crustal structure of the Carnegie Ridge, Panama Basin and Cocos Ridge, MS thesis. University of Hawaï, Honolulu

Bialas J, Flueh ER, Borhmann G, The Paganini Scientific Party (1999) Cruise report SO144 Paganini, pp. 437 pages, GEOMAR, Kiel

Birch F (1961) The velocity of compressional waves in rocks to 10 kilobars, part 2. J Geophys Res 66:2199–2224

Bjarnason IT, Menke W, Flovenz OG, Caress D (1993) Tomographic image of the mid-Atlantic plate boundary in Southwestern Iceland. J Geophys Res 98(B4):6607–6622

de Boer J, Defant MJ, Steward RH, Restrepo JF, Clark LF, Ramirez A (1988) Quartenary calc-alkaline volcanism in Western Panama: regional variation and implication for plate tectonic framework. J South Am Earth Sci 1:275–293

Callot JP, Grigné C, Geoffroy L, Brun JP (2001) Development of volcanic passive margins: two dimensional laboratory models. Tectonics 20(1):148–159

Carlson RL, Herrick CN (1990) Densities and porosities in the oceanic crust and their variations with depth and age. J Geophys Res 95:9153–9170

Carlson RL, Raskin GS (1984) Density of the oceanic crust. Nature 311:555–558

Charvis P, Operto S (1999) Structure of the Cretaceous Kerguelen Volcanic Province (southern Indian Ocean) from wide-angle seismic data Journal of Geodynamics, special issue ''Hotspot and oceanic crust interaction'', Ph. Charvis and J. J Dañobeitia editors 28(1):51–71

Charvis P, Recq M, Operto S, Bréfort D (1995) Deep structure of the northern Kerguelen-Plateau and hot spot-related activity. Geophys J Int 122(3):899–924

Coffin MF, Eldholm O (1994) Large igneous provinces: crustal structure, dimensions, and external consequences. Rev Geophys 32(1):1–36

Collot J-Y, Charvis P, Gutscher MA, Operto S (2002) Exploring the Ecuador-Colombia active margin and interplate seismogenic zone. EOS, Trans Am Geophys Union 83(17):189–190

Eldholm O (1991) Magmatic-tectonic evolution of a volcanic rifted margin. Mar Pet Geol 102:43–61

Gardner TW, Verdonck D, Pinter NM, Slingerland R, Furlong KP, Bullard TF, Wells SG (1992) Quaternary uplift astride the aseismic. Cocos Ridge, Pacific Coast, Costa Rica Geol Soc Am Bull 104:219–232

Geoffroy L, Gélard JP, Lepvrier C, Olivier P (1998) The coastal flexure of disko (west Greenland) onshore expression of the oblique reflectors. J Geol Soc Lond 155:463–473

Hamilton EL (1978) Sound velocity-density relations in seafloor sediments and rocks. J Acoust Soc Am 63:366–377

Hardy NC (1991) Tectonic evolution of the Easternmost Panama Basin: some new data and interferences. J South Am Earth Sci 4(3):261–269

Hey RN (1977) Tectonic evolution of the Cocos-Nazca spreading centre. Geol Soc Am Bull 88:1414–1420

Hinz K (1981) A hypothesis on terrestrial catastrophes: wedges of very thick oceanward dipping layers beneath passive margins - Their origin and paleoenvironments significance. Geol Jahrb 22:345–363

Hoernle K, van de Bogaard P, Werner R, Lissina B, Hauff F, Alvarado G, Garbe-Schönberg D (2002) Missing history (16–71 Ma) of the Galapagos Hotspot: implications for the tectonic and biological evolution of the Americas. Geology 30(9):795–798

Johnson GL, Lowrie A (1972) Cocos and Carnegie Ridges - result of the Galapagos ''hot spot''? Earth Planet Sci Lett 14:279–280

Jordan TH (1975) The present-day motions of the Caribbean plate. J Geophys Res 80:4433–4439

Kellogg JN, Vega V (1995) Tectonic development of Panama, Costa Rica, and the Colombian Andes: constraints from global positioning system geodetic studies and gravity. Geol Soc Am Bull 295(Special Paper):7590

Lonsdale PF (2005) Creation of the Cocos and Nazca Plates by fission of the Farallon. Plate Tectonophys 404:237–264

Lonsdale P, Klitgord KD (1978) Structure and tectonic history of the Eastern Panama Basin. Geol Soc Am Bull 89:981–999

McCarthy J, Mutter JC, Morton JL, Sleep NH, Thompson GA (1988) Relic magma chamber structures preserved within the Mesozoïc North Atlantic Crust. Geol Soc Am Bull 100:1423–1436

Meschede M, Barckhausen U, Worm HU (1998) Extinct spreading on the Cocos. Ridge Terra Nova 10:211–216

Molnar P, Sykes LR (1969) Tectonics of the Caribbean and Middle American region from focal mechanisms and seismicity. Bull Geol Soc Am 80:1639–1684

Mutter JC (1985) Seaward dipping reflectors and the Continent-Ocean boundary at passive continental margins. Tectonophysics 114:117–131

Mutter CZ, Mutter JC (1993) Variations in thickness of layer 3 dominate oceanic crustal structure. Earth Planet Sci Lett 117:295–317

Mutter JC, Talwani M, Stoffa PL (1982) Origin of seaward-dipping reflectors in oceanic crust off the Norwegian margin by subaerial sea-floor spreading. Geology 10:353–357

Palmason G (1980) A continuum model of crustal generation in Iceland: Kinematics aspects. J Geophys 47:7–18

Pennington WD (1981) Subduction of the Eastern Panama Basin and seismotectonics of Northwestern. South Am J Geophys Res 86:10753–10770

Sallares V, Charvis P (2003) Seismic constraints on the Geodynamic evolution of the Galapagos province. Earth Planet Sci Lett 214:545–559

Sallares V, Charvis P, Flueh ER, Bialas J (2003) Seismic structure of Cocos and Malpelo volcanic Ridges and implications for Hotspot-Ridge Interaction. J Geophys Res 108(B12):2564, DOI: 10.01029/2003JB002431

Sandwell DT, Smith WHF (1997) Marine gravity anomaly from Geosat and ERS 1 satellite altimetry. J Geophys Res 102(B5):10039–10054

Schlich R, Rotstein Y, Schaming M (1993) Dipping basement reflectors along volcanic passive margins - new insight using data from the Kerguelen. Plateau Terra Nova 5:157–163

Silver EA, Reed DL, Tagudin JE, Heil DJ (1990) Implications of the north and south Panama thrust belts for the origin of the Panama orocline. Tectonics 9(2):261–281

Taboada A, Rivera LA, Fuenzalida A, Cisternas A, Philip H, Bijwaard H, Olaya J, Rivera C (2000) Geodynamics of the Northern Andes: subductions and intracontinental deformation (Colombia). Tectonics 19(5):787–813

Talwani M, Worzel JL, Landisman M (1959) Rapid gravity computations for two-dimensional bodies with application to the Mendocino submarine fracture zone. J Geophys Res 64:49–61

Tard F, Masse P, Walgenswitz F, Grüneisen P (1991) The volcanic passive margin in the vicinity of Aden, Yemen Bulletin du Centre de Recherche d'Exploration et de Production de Elf. Aquitaine 15:1–9

Van Andel TH, Heath GR, Malfait BT, Heinrichs DF, Ewing JI (1971) Tectonics of the Panama Basin, Eastern Equatorial Pacific. Geol Soc Am Bull 82:1489–1508

Wade US, Lister CRB, Lewis BTR (1977) Seismic refraction over Malpelo Ridge in the Panama Basin. In: Ramirez JE, Aldrich LT (eds) Inst Geofisico the ocean transition in SW Colombia. Universidad Javeriana, Bogota, pp 209–216

Werner R, Hoernle K, van den Bogaard P, Ranero CR, von Huene R, Korich D (1999) Drowned 14-m.y.-old Galapagos archipelago off the coast of Costa Rica: implications for tectonic and evolutionary models. Geology 27(6):499–502

Werner R, Hoernle K, Barckhausen U, Hauff F (2003) Geodynamic evolution of the Galapagos hot spot system (Central East Pacific) over the past 20 m.y.: constraints from morphology, geochemistry, and magnetic anomalies Geochemistry, Geophysics and Geosystems 4(12):DOI:10.1029/2003GC000576

White RS (1992) Crustal structure and magmatism of North Atlantic continental margins. J Geol Soc Lond 149:841–854

White RS, McBride JH, Henstock TJ, Hobbs RW (1994) Internal structure of a spreading segment of Mesozoic crust. Geology 22:597–600

Zelt CA, Smith RB (1992) Seismic traveltime inversion for 2D crustal velocity structure. Geophys J Int 108:16–34